https://doi.org/10.15407/ujpe71.3.210

G. MURODOV,[1] I. DOROSHENKO,[1,2] H. HUSHVAKTOV,[1] U. KHUJAMOV,[1]
G. NURMURODOVA [1]

[1] Institute of Engineering Physics, Sharof Rashidov Samarkand State University
(Uzbekistan; e-mail: gnurmuradava@gmail.com)
[2] Taras Shevchenko National University of Kyiv
(64/13, Volodymyrska Str., Kyiv 01601, Ukraine)

WEAK HYDROGEN BONDING IN $CD_3Hal \cdots HCl$ COMPLEXES: IR SPECTROSCOPY AND MP2 CALCULATIONS

The formation and vibrational properties of $CD_3Hal \cdots HCl$ complexes ($Hal = F$, Cl, Br) were investigated in liquid argon at 120 K using infrared (IR) spectroscopy and anharmonic frequency calculations at the MP2/6-311++G(3df,3pd) level. Upon complex formation, the $\nu(HCl)$ stretching band exhibited systematic red shifts, increasing from CD_3F to CD_3Br, accompanied by band narrowing due to reduced rotational freedom of the bound HCl. For the $CD_3F \cdots HCl$ complex, additional red shifts of 16 and 12 cm^{-1} were observed in the $\nu(CF)$ and $\nu_\beta(CD_3)$ modes, respectively, in agreement with the computed results. Charge distribution analysis revealed geometry changes consistent with non-linear complex structures. Force constants and reduced masses were calculated to rationalize spectral intensity variations. Atoms in Molecules (AIM) topological analysis confirmed weak hydrogen bonds with energies ranging from 2.6 to 5.5 $kcal \cdot mol^{-1}$, correlating with the halogen electronegativity ($F > Cl > Br$). The agreement between experimental and theoretical data highlights the relationship between vibrational shifts, bond strength, and electronic structure in weakly hydrogen-bonded systems.

Keywords: deuterated methyl halides, hydrogen bond, infrared spectroscopy, liquid argon, MP2 calculations, spectral shifts, weak intermolecular interactions.

1. Introduction

Hydrogen bonding is one of the most fundamental phenomena in molecular physics and spectroscopy, strongly influencing the structure, dynamics, and physicochemical properties of molecules. While strong hydrogen bonds have been extensively studied, weak hydrogen bonds have attracted increasing attention [1–6] because they manifest through subtle spectral shifts and reflect a delicate balance of electrostatic, inductive, and dispersion forces.

Inert solvents such as liquefied Ar, Kr, and Xe are widely employed in the study of weak hydrogen bonding, as they provide high transparency and minimize intermolecular interactions while allowing for sharp spectral lines [7–9]. Moitra and co-workers [10], as well as Latajka *et al.* [11], demonstrated that the shape and width of ν(AH) bands in cryogenic matrices depend strongly on the solvent environ-

Citation: Murodov G., Doroshenko I., Hushvaktov H., Khujamov U., Nurmurodova G. Weak hydrogen bonding in $CD_3Hal \cdots HCl$ complexes: IR spectroscopy and MP2 calculations. *Ukr. J. Phys.* **71**, No. 3, 210 (2026). https://doi.org/10.15407/ujpe71.3.210.

ment. Similarly, Herrebout and collaborators investigated DCl oligomers in liquid Ar and Kr and identified dimers, trimers, and tetramers with distinct vibrational features [12].

Halogen-containing complexes have also been the subject of extensive research. Szostak *et al.* observed a significant red shift in the ν(HCl) band of the methylenecyclopropane $\cdots$ HCl complex in argon [13], while Andrews and co-workers studied the infrared spectrum of the H_3N–HCl complex in solid Ne, Ne/Ar, Ar, and Kr was studied, as well as the matrix effect on the hydrogen-bonded complex [14]. Anharmonic effects in CF_3Br within liquid argon were also explored by Zhigula *et al.* [15].

Theoretical methods complement experimental investigations. Howard *et al.* studied anharmonic vibrational frequencies in hydrogen-bonded dimers such as $(HF)_2$ and $(H_2O)_2$ using high-level computational methods, showing good agreement with experiment [16]. Riley and co-workers [17], as well as Bachorz *et al.* [18], assessed the applicability of MP2 and related methods for describing noncovalent interactions, providing important benchmarks for interpreting IR spectra of weak complexes.

Topological approaches have further advanced the field. Bader's Atoms in Molecules (AIM) theory allows hydrogen bonds to be characterized through electron density analysis [19]. Espinosa and colleagues demonstrated correlations between bond critical point parameters ($\rho(r_{\mathrm{BCP}})$, $\nabla^2\rho(r_{\mathrm{BCP}})$) and hydrogen bond strength [20, 21]. Grabowski also provided an in-depth discussion of covalency contributions in hydrogen bonding [22].

More recent studies have highlighted the interplay between halogen bonding and hydrogen bonding. Politzer *et al.* [23] and Cavallo *et al.* [24] showed that σ-hole interactions can compete with hydrogen bonding, significantly influencing spectral properties.

Thus, both experimental and theoretical investigations in recent years have revealed the complex nature of weak hydrogen bonds. In this work, we examine $CD_3Hal\cdots HCl$ (Hal = F, Cl, Br) complexes in liquid argon (120 K) using infrared spectroscopy and MP2/6-311++G(3df,3pd) calculations combined with AIM analysis. The aim is to assess how the halogen nature influences hydrogen bond strength, vibrational shifts, and electronic density topology.

2. Methods

2.1. Experimental method

Infrared absorption spectra of free molecules (HCl, CD_3F, CD_3Cl, CD_3Br) and their complexes with HCl were recorded in liquid argon at 120 K. Mixtures of $CD_3Hal + HCl$ (Hal = F, Cl, Br) were prepared at concentrations of (2–3) $\times 10^{-4}$ mol/L in high-purity argon (99.999%) using cryogenic techniques. The spectra were measured with a Bruker IFS-125 HR FTIR spectrometer, operating in the 3200–900 cm^{-1} range, which includes ν(HCl), $\nu_\beta(CD_3)$, ν(CF), and $\nu_{ass}(CD_3)$ bands. Each spectrum was averaged over 64 scans with a resolution of 0.01 cm^{-1}. The temperature was controlled to ± 3 K using Pt-100 sensors.

Complex formation was monitored through systematic red shifts of the ν(HCl) band, as well as perturbations in the CD_3Hal vibrational modes. Concentration variations and line half-widths ($\Delta\nu_{1/2}$) were used to distinguish between monomer and complex contributions [25–28].

3. Computational Details

Quantum-chemical calculations were carried out with Gaussian 16 Revision C.01 [29]. Vibrational frequencies were obtained at the MP2/6-311++G(3df,3pd) level, which includes diffuse and polarization functions, ensuring a reliable description of weak noncovalent interactions [30–32]. Anharmonic corrections were applied to improve agreement with experiment.

The argon matrix environment was approximated in these calculations. Molecular visualizations and vibrational mode assignments were performed using GaussView 6.1 and Chemcraft [33, 34]. Topological analysis of electron density was conducted using Bader's Atoms in Molecules (AIM) [35] approach with the Multiwfn and VMD programs [36, 37].

4. Results and Discussions

4.1. Vibrational Shifts in ν(HCl) Bands

Among molecules capable of forming weak hydrogen bonds, hydrogen halides occupy a distinctive position. Fluoromethane, in particular, has long been recognized as a very weak proton acceptor and represents one of the earliest systems investigated in this context. In our previous work, krypton (Kr) and xenon (Xe) were used as cryogenic media to study the

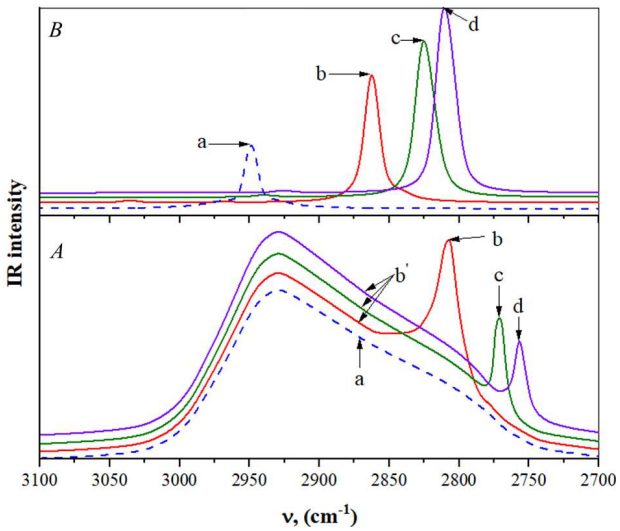

Fig. 1. Absorption spectra of the ν(HCl) stretching band in argon at 120 K (A): (a) free HCl, (b) HCl + CD_3F, (c) HCl + + CD_3Cl, and (d) HCl + CD_3Br. The sharp bands of the complexes appear on the P-branch side of the free HCl line. Corresponding spectra calculated using anharmonic vibrational frequency approximations (B)

$(CH_3)_2CO \cdots HCl$ complex, where the ν(HCl) stretching band was thoroughly characterized [38]. These findings provide a useful reference for interpreting the spectral shifts observed in the present $CD_3Hal \cdots HCl$ complexes.

In the present study, we extend these investigations to isotopically substituted $CD_3HalHCl$ (Hal = F, Cl, Br) complexes, focusing on the vibrational features of the ν(HCl) stretching band and on the spectral manifestation of hydrogen bonding in the vibrational bands of the proton acceptor. The substitution of hydrogen by deuterium in the CD_3 group results in a downshift of the ν(CD) stretching band relative to the ν(CH) band, which facilitates a more reliable observation of the ν(HCl) absorption in the IR spectrum. For this reason, the CD_3Hal series was selected for detailed analysis.

The proton-accepting ability of the halogenated isotopologues, which reflects the hydrogen-bond strength, decreases in the order $CD_3F \rightarrow CD_3Cl \rightarrow$ $\rightarrow CD_3Br$ [39, 40]. For all three complexes isolated in liquid argon, the ν(HCl) stretching band exhibits a distinct red shift relative to the free HCl line, analogous to the behavior previously reported for $CH_3F \cdots HCl$. These shifted absorption features are observed in the P-branch region of free HCl (Fig. 1, A). At 120 K, sharp ν(HCl) bands with half-widths of approximately $\Delta\nu_{1/2} \approx 10$ cm^{-1} were detected at 2804, 2770, and 2756 cm^{-1} for the CD_3F, CD_3Cl, and CD_3Br complexes, respectively (Fig. 1, A).

Anharmonic vibrational frequency calculations provide further support for these assignments, predicting the ν(HCl) stretching frequencies at 2859.55, 2823.68, and 2813.97 cm^{-1} for $CD_3F \cdots HCl$, $CD_3Cl \cdots HCl$, and $CD_3Br \cdots HCl$, respectively (Fig. 1, B). The experiments were conducted at 120 K, since CD_3Cl and particularly CD_3Br exhibit poor solubility under cryogenic conditions.

In Fig. 1, A, bands a and b' correspond to free HCl molecules present in the mixture. Since the HCl molecules undergo rovibrational motion freely in the argon medium, the characteristic P-, R-, and Q-branches are observed. In Fig. 1, B, the same bands were reproduced using anharmonic approximations, with argon chosen as the solvation environment.

The observed narrowing of the ν(HCl) band can be rationalized by two competing effects. On the one hand, hydrogen-bond formation typically leads to band broadening. On the other hand, in the $CD_3Hal \cdots HCl$ complex the band becomes narrower due to the slowdown of rotational motion, which arises from the increased moment of inertia compared with free HCl. Because the hydrogen bond energy in these complexes is relatively low ($E_{HB} \sim 1$ kcal/mol), distortion of the proton-donor band is not significant, resulting in the observed narrowing of the ν(HCl) band.

A noteworthy feature is that the red shift of the ν(HCl) band increases as the hydrogen bond strength decreases, i.e., when moving from C–F to C–Br. As illustrated in Fig. 1, with decreasing hydrogen-bond strength, the concentration of complexes decreases, while the red shift of the ν(HCl) band increases from 65 to 114 cm^{-1}. Due to the poor solubility of CD_3Cl and CD_3Br, it was not possible to determine their hydrogen bond energies experimentally. For the $CD_3F \cdots HCl$ complex, the experimentally determined hydrogen bond energy (E_{HB}) was found to be the same as that of $CH_3F \cdots HCl$, amounting to 1.1 kcal/mol.

Similar results have been reported in the literature [39, 40]. For example, in phenol + $C_7H_{15}F$ (Cl, Br, I) systems, the hydrogen bond energy decreases from 2.1 to 1.2 kcal/mol, while the red shift of the ν(OH)

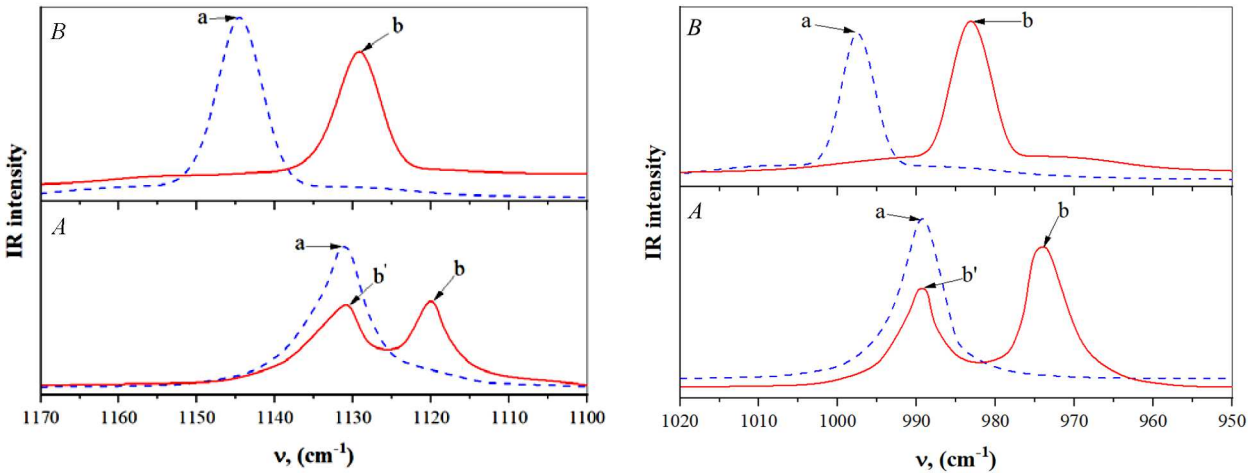

a *b*

Fig. 2. Absorption spectra (A) of CD_3F (a) and a $CD_3F + HCl$ mixture (b) in liquid argon. Calculated spectra (B) using anharmonic approximations. Vibrational assignments: $\nu_\beta(CD_3)$ (left) and $\nu(CF)$ (right)

Table 1. **Selected vibrational frequencies (ν cm^{-1}) of free CD_3F and the $CD_3F\cdots HCl$ complex in liquid argon, obtained from experimental spectra and anharmonic calculations. The corresponding frequency shifts ($\Delta\nu$) are also presented**

Vibrational frequencies	ν, (cm^{-1})				$\Delta\nu$, (cm^{-1})	
	Free molecule		Complex		Free molecule	
	Exp.	Calc.	Exp.	Calc.	Exp.	Calc.
ν(CF)	991 ± 2	997.92	975 ± 2	982.09	16	15.83
$\nu_\beta(CD_3)$	1132 ± 3	1144.87	1120 ± 3	1129.96	12	14.91
$\nu_s(CD_3)$	2088 ± 2	2114.65	2088	2112.01	0	2.64
$\nu_{ass}(CD_3)$	2258 ± 2	2302.04	2269 ± 3	2304.88	–11	–2.84

Note: ν(HCl) and ν(CF) – stretching, $\nu_\beta(CD_3)$ – bending (in – plane), $\nu_s(CD_3)$ – symmetric stretching, $\nu_{ass}(CD_3)$ – antisymmetric stretching, Exp. – experiment, Calc. – calculations, $\Delta\nu = \nu_{monomer} - \nu_{complex}$.

band increases from 40 to 70 cm^{-1}. A comparable trend was observed in argon matrices at 20 K for the transition from $CH_3F\cdots HCl$ to $CH_3Cl\cdots HCl$, where the ν(HCl) bands of the complexes appeared at 2793 and 2745 cm^{-1}, respectively [41]. In this case, the ν(HCl) frequency was substantially lower than in argon solutions. The unusual behavior of the proton-donor bands remains unexplained. Nevertheless, in such systems the $E_{HB} \sim \Delta\nu$ correlation cannot be reliably applied to determine hydrogen bond energies.

4.2. Effect on acceptor vibrations (CD_3Hal modes)

With regard to the bands of the acceptor molecules, a noticeable distortion is observed only in the case of CD_3F, where weak hydrogen bonding leads to significant spectral changes. Similar to CH_3F, the ν(CF) stretching band of the free molecule undergoes a red shift from 991 cm^{-1} to 975 cm^{-1} upon complex formation. The calculations predict a comparable decrease in frequency, from 997.92 to 982.09 cm^{-1} (Fig. 2). Experimentally, the half-width of this band was also found to decrease from 8 to 6 cm^{-1}.

The frequency values of these bands are summarized in Table 1. Experimentally, the ν(CF) band of CD_3F exhibited a frequency shift of $\Delta\nu = 16$ cm^{-1}, while the calculations predicted a nearly identical value of 15.83 cm^{-1}.

In Fig. 3, the $\nu_{ass}(CD_3)$ stretching vibration of CD_3F demonstrates a distinct blue shift upon complexation with HCl. This behavior contrasts with

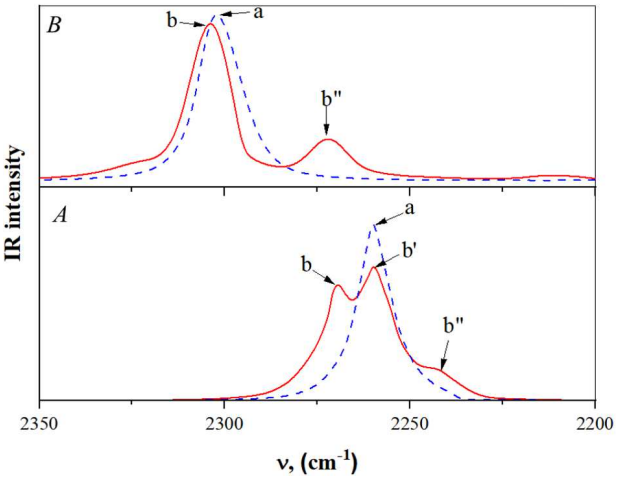

Fig. 3. Absorption spectra (A) of the $\nu_{\text{ass}}(CD_3)$ stretching band in liquid argon: (a) free CD_3F, (b) CD_3F + HCl mixture, (b') free CD_3F molecules present in the mixture, and (b'') overtone band of the $\nu_\beta(CD_3)$ vibration. Calculated spectra (B) obtained using anharmonic frequency approximations, confirming the assignment of the b'' band to the $\nu_\beta(CD_3)$ overtone

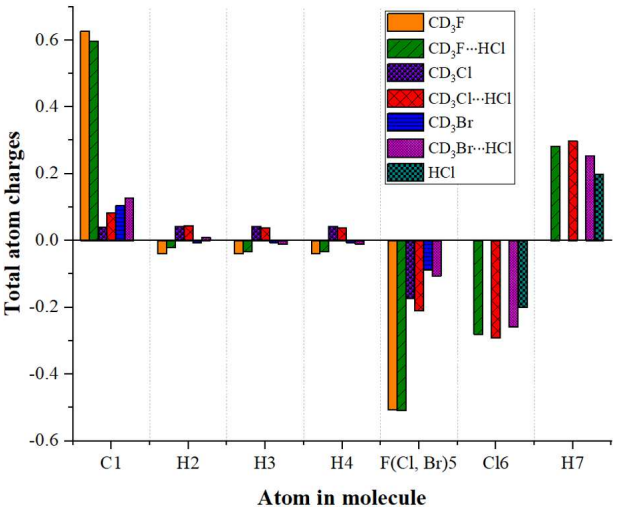

Fig. 4. Schematic representation of the total atomic charge distribution for the studied complexes

the more commonly observed red shift in hydrogen-bonded systems and can be attributed to changes in the rotational dynamics of the molecule. Specifically, the width of the perpendicular $\nu_{\text{ass}}(CD_3)$ band, which is governed by the rotational constant around the C_3 axis, decreases upon complex formation, indicating a restriction in rotational motion.

As shown in Fig. 3, A, the a band corresponds to the $\nu_{\text{ass}}(CD_3)$ vibration of the free CD_3F molecule, while the b band represents the same vibration within the $CD_3F \cdots HCl$ complex. The b' band arises from uncomplexed CD_3F molecules remaining in the mixture, confirming the coexistence of both free and complexed species under the experimental conditions. Additionally, the b'' band is assigned to the overtone of the $\nu_\beta(CD_3)$ vibration. This assignment is validated by the anharmonic vibrational frequency calculations shown in Fig. 3, B, which reproduce the position of the overtone band with good accuracy.

These findings indicate that hydrogen bonding in the $CD_3F \cdots HCl$ system not only perturbs the proton donor (HCl) vibrations but also leads to measurable spectral changes in the acceptor molecule, particularly through modifications of the C–D stretching modes.

In contrast to the asymmetric stretching mode, the $\nu_s(CD_3)$ vibration shows almost no spectral shift in the experimental spectra upon complex formation. This indicates that the symmetric stretching mode of the CD_3 group is only weakly perturbed by the hydrogen-bonding interaction. However, anharmonic frequency calculations (Table 1) predict a slight red shift of about 2.64 cm^{-1} for this vibration, suggesting that the effect of complexation is too small to be unambiguously resolved under the experimental resolution.

4.3. Charge redistribution and structural changes

Charge distribution analysis (Figure 4, Table 2) revealed significant electron density redistribution upon complex formation. The halogen atom (F, Cl, Br) acquired a more negative charge, while the H atom in HCl became more positive, consistent with the hydrogen bond formation. These changes directly influenced bond lengths: for instance, the $F \cdots H$ distance in $CD_3F \cdots HCl$ was calculated as 1.914 Å, compared to 2.338 Å ($Cl \cdots H$) and 2.492 Å ($Br \cdots H$) in the corresponding complexes (Table 4).

Geometric optimization (Figure 5) confirmed that all complexes adopt non-linear structures, with the ∠F–H–Cl angle deviating significantly from 180° (166.5° for $CD_3F \cdots HCl$, 161.8° for $CD_3Cl \cdots HCl$, and 160.2° for $CD_3Br \cdots HCl$). These distortions further evidence the weak and flexible nature of these hydrogen bonds.

Table 2. **Total atomic charges of the free molecules and their complexes**

Atom	Free molecule	Complex	Atom	Free molecule	Complex	Atom	Free molecule	Complex
C1	0.627	0.597	C1	0.041	0.083	C1	0.104	0.127
D2	–0.040	–0.022	D2	0.044	0.045	D2	–0.006	0.009
D3	–0.040	–0.034	D3	0.044	0.038	D3	–0.006	–0.011
D4	–0.040	–0.034	D4	0.044	0.038	D4	–0.006	–0.011
F5	–0.506	–0.509	Cl5	–0.175	–0.210	Br5	–0.087	–0.107
Cl6	–0.201	–0.280	Cl6	–0.201	–0.292	Cl6	–0.201	–0.261
H7	0.201	0.282	H7	0.201	0.297	H7	0.201	0.255

Note: The total atomic charges were obtained from the population analysis at the MP2/6-311++G(3df,3pd) level of theory. All values are given in atomic units (a.u.).

To assess the influence of hydrogen bonding on spectral parameters such as frequency and intensity, the mechanical and electro-optical properties of the $CD_3F\cdots HCl$ complex were analyzed. The calculations were performed using the equilibrium geometry corresponding to the lowest-energy structure (Fig. 5). Structural changes induced by weak hydrogen bond formation were considered, and the resulting bond lengths and angles are summarized in Table 3.

4.4. Force constants and reduced masses

Force constant analysis (Table 4) revealed a general decrease in bond stiffness upon hydrogen bond formation, particularly for ν(HCl) and ν(CF) modes. For instance, the K^a(HCl) force constant decreased from 9.005×106 cm^{-1} in the free molecule to $8.401 \times \times 106$ cm^{-1} in $CD_3F\cdots HCl$. Reduced masses were also modified, reflecting coupling between donor and acceptor vibrations.

These parameters were obtained from vibrational analyses at the MP2/6-311++G(3df,3pd) level of theory. The force constants characterize the stiffness of the corresponding vibrational modes, while the reduced masses determine the effective inertia of the vibrations. Together, they provide a basis for evaluating vibrational frequencies and for analyzing the effect of weak hydrogen bonding on the mechanical properties of the complexes.

The mixing of vibrational modes was further confirmed by normal coordinate analysis (Table 7). In CD_3F, the ν(CF) vibration was strongly coupled with $\nu_\beta(CD_3)$, and this coupling persisted, albeit more weakly, in the complex. This explains why both ν(CF) and $\nu_\beta(CD_3)$ bands exhibit significant red shifts, while $\nu_s(CD_3)$ remains largely unaffected.

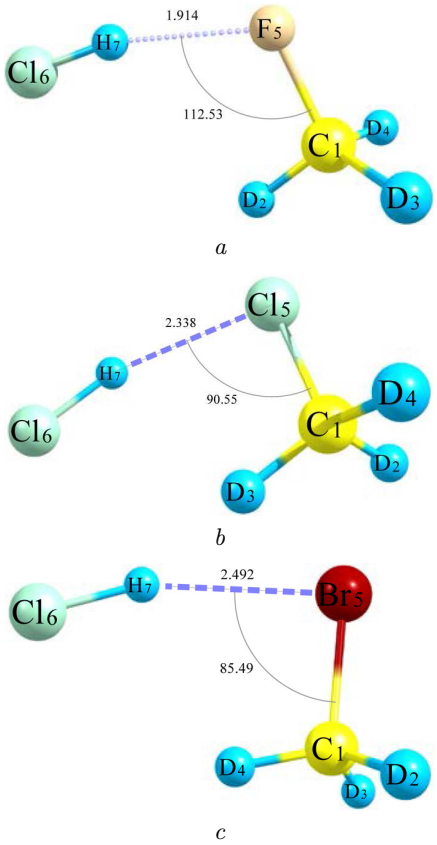

Fig. 5. Optimized geometries of the $CD_3F\cdots HCl$, $CD_3Cl\cdots HCl$, and $CD_3Br\cdots HCl$ complexes calculated at the MP2/6-311++G(3df,3pd) level. Intermolecular features are highlighted, with hydrogen bond lengths and key angles indicated

For the $CD_3F\cdots HCl$ complex, the spectral parameters undergo noticeable changes as a result of the intermolecular interactions. Quantum chemical calcula-

Table 3. **Bond lengths and bond angles between the atoms of the free molecules and their complexes**

Molecules	Bond lengths, (Å)		Bond angles, (°)		Molecules	Bond lengths, (Å)		Bond angles, (°)	
HCl	r(H–Cl)	1.272	–	–	$CD_3Cl\cdots HCl$	r(C1–D2)	1.083	βD2C1D3	110.61
CD_3F	r(C1–D2)		βD2C1D3	110.26		r(C1–D3)	1.084	βD2C1D4	110.78
	r(C1–D3)	1.086	βD2C1D4			r(C1–D4)	1.083	βD3C1D4	110.61
	r(C1–D4)		βD3C1D4	110.25		r(C1–Cl5)	1.778	βD2C1Cl5	108.18
	r(C1–F5)	1.385	βD2C1F5	108.68		r(Cl5$\cdots$H7)	2.338	βD3C1Cl5	108.39
			βD3C1F5			r(Cl6–H7	1.282	βD4C1Cl5	108.17
			βD4C1F5	108.67				βC1Cl5H7	90.55
$CD_3F\cdots HCl$	r(C1–D2)	1.086	βD2C1D3	110.67				βCl5H7Cl6	161.78
	r(C1–D3)	1.085	βD2C1D4		CD_3Br	r(C1–D2)	1.083	βD2C1D3	
	r(C1–D4)		βD3C1D4	110.82		r(C1–D3)		βD2C1D4	110.83
	r(C1–F5)	1.396	βD2C1F5	108.35		r(C1–D4)		βD3C1D4	
	r(F5$\cdots$H7)	1.914	βD3C1F5	108.11		r(C1–Br5)	1.931	βD2C1Br5	
	r(C16–H7)	1.281	βD4C1F5					βD3C1Br5	108.07
			βC1F5H7	112.53				βD4C1Br5	
			βF5H7C16	166.47	$CD_3Br\cdots HCl$	r(C1–D2)	1.082	βD2C1D3	111.18
CD_3Cl	r(C1–D2)	1.083	βD2C1D3	110.38		r(C1–D3)		βD2C1D4	111.06
	r(C1–D3)		βD2C1D4			r(C1–D4)	1.083	βD3C1D4	
	r(C1–D4)		βD3C1D4			r(C1–Br5)	1.935	βD2C1Br5	107.75
	r(C1–Cl5)	1.773	βD2C1Cl5			r(Br5$\cdots$H7)	2.492	βD3C1Br5	107.74
			βD3C1Cl5	108.55		r(Cl6–H7)	1.282	βD4C1Br5	107.87
			βD4C1Cl5					βC1Br5H7	85.49
								βBr5H7Cl6	160.21

N o t e: The values correspond to the optimized geometries of the free molecules and their hydrogen-bonded complexes at the MP2/6-311++G(3df,3pd) level of theory.

Table 4. **Calculated force constants (106 cm^{-2}) and reduced masses (amu) in the Ar environment**

Molecules	Force constant	Free molecules	Complex	Reduced mass	Free molecules	Complex
HCl	K^a(HCl)	9.005	8.401	M^a(HCl)	1.0360	1.0364
CD_3F	K^a(CF)	1.013	0.979	M^a(CF)	4.1372	4.8261
	$K^a_\beta(CD_3)$	1.336	1.304	$M^a_\beta(CD_3)$	3.6212	3.2222
	$K^a_s(CD_3)$	4.673	4.68	$M^a_s(CD_3)$	2.1003	2.0972
	$K^a_{\rm ass}(CD_3)$	5.465	5.497	$M^a_{\rm ass}(CD_3)$	2.3996	2.4022
HCl	K^b(HCl)	9.005	8.216	M^b(HCl)	1.0360	1.0366
CD_3Cl	K^b(CF)	0.534	0.524	M^b(CF)	6.1614	6.3355
	$K^b_\beta(CD_3)$	1.119	1.153	$M^b_\beta(CD_3)$	2.6894	2.6504
	$K^b_s(CD_3)$	4.855	4.865	$M^b_s(CD_3)$	2.0987	2.0971
	$K^b_{\rm ass}(CD_3)$	5.546	5.572	$M^b_{\rm ass}(CD_3)$	2.3905	2.3914
HCl	K^c(HCl)	9.005	8.17	M^c(HCl)	1.0360	1.0366
CD_3Br	K^c(CF)	0.365	0.36	M^c(CF)	5.4082	5.4612
	$K^c_\beta(CD_3)$	1.047	1.055	$M^c_\beta(CD_3)$	2.6675	2.6392
	$K^c_s(CD_3)$	4.864	4.875	$M^c_s(CD_3)$	2.0936	2.0920
	$K^c_{\rm ass}(CD_3)$	5.584	5.61	$M^c_{\rm ass}(CD_3)$	2.3899	2.3909

tions revealed the following hydrogen bond characteristics: the F ⋯ H distance is r(F ⋯ H) = 1.914 Å, the corresponding bond force constant is $K_\sigma = 0.019 \times$ $\times 106$ cm^{-1}, and the vibrational frequency of the F ⋯ H bond is $\nu_\sigma = 72.84$ cm^{-1}. These values indicate the formation of a weak but well-defined hydrogen bond, consistent with the observed red shift in the ν(HCl) stretching vibration.

4.5. Integrated absorption coefficients and intensities

Experimental integrated absorption coefficients (Table 5) demonstrated that complexation leads to decreased intensity of the $\nu_\beta(CD_3)$ and $\nu_{as}(CD_3)$ modes, while ν(CF) remains nearly unchanged. The ν(HCl) band exhibited strong absorption ($86 \times$ $\times 10^{-8}$ cm^{2}s^{-1}mol^{-1}), consistent with its donor character and alignment along the hydrogen bond axis.

The absorption coefficient values obtained in this way, considering the experimental uncertainties, are presented in Table 5.

The absorption coefficients characterize the intensity of the vibrational bands, while the half-width values provide information about line-broadening effects. Both parameters were used to analyze the influence of weak hydrogen bonding on the spectroscopic properties of the complexes.

Electro-optical analysis (Tables 6–7) supported these findings. The calculated transition dipole derivatives indicated that the $\nu_\beta(CD_3)$ band loses intensity upon complexation, while ν(CF) gains intensity. Slight discrepancies between theoretical and experimental intensities may arise from the assumption of a linear complex model in calculations, whereas the real structures are non-linear.

The coefficients describe the displacement amplitudes of the atoms along each normal coordinate, providing insight into the vibrational coupling within the complex.

These parameters characterize the changes in molecular dipole moments and polarizabilities upon complex formation, providing a quantitative measure of the electro-optical effects induced by weak hydrogen bonding.

4.6. AIM topological analysis of hydrogen bonds

Atoms in Molecules (AIM) analysis provided direct evidence of weak hydrogen bond formation (Figure 6, Table 8). The electron density at the bond critical point ($\rho(r_{BCP})$) decreased in the order F (0.0220 a.u.) > Cl (0.0184 a.u.) > Br (0.0166 a.u.), consistent with halogen electronegativity.

Table 5. **Experimental and calculated absorption coefficients (A) and half-widths ($\Delta\nu_{1/2}$) for the free CD_3F molecule and the $CD_3F + HCl$ mixture in the Ar environment**

Vibrational frequencies	A, 10^{-8} cm^2/s$^{-1}\cdot$ mol^{-1}				$\Delta\nu_{1/2}$, cm^{-1}			
	Free molecules		Complex		Free molecules		Complex	
	Exp.	Calc.	Exp.	Calc.	Exp.	Calc.	Exp.	Calc.
ν(CF)	41	59	43 ± 3	71	8	8.09	6	7.99
$\nu_\beta(CD_3)$	27 ± 3	33	10 ± 2	23	11	9.50	6	9.10
$\nu_s(CD_3)$	15 ± 3	11		10	9			
$\nu_{ass}(CD_3)$	28 ± 3	13	12 ± 3	10	17	9.75	13	10.13

Table 6. **Normal vibration mode coefficients of the $CD_3F\cdots HCl$ complex (in Å)**

Variables	Q_1	Q_2	Q_3	Q_4	Q_5
			CD_3F		
q_1	0.093	0.019	–0.015	–	–
q_2	–0.031	0.103	–0.046	–	–
q_3	–0.010	0.038	0.045	–	–
			$CD_3F\cdots HCl$		
q_1	0.089	0.021	–0.013	0	0
q_2	–0.027	0.126	–0.035	0	0
q_3	–0.010	0.025	0.051	0	0
q_4	0	0.003	–0.028	0.170	0.107
q_5	0	0	0	0	0.113

Table 7. **Calculated electro-optical parameters for free molecules and complexes**

ν	Free molecule $\left(\frac{\partial\mu_j}{\partial q_j}\right)_0$, D	$\left(\frac{\partial\mu_j}{\partial q_j}\right)_0$, D/Å	Complex $\left(\frac{\partial\mu}{\partial Q_i}\right)_0$, D
$\nu_s(CD_3)$	0.103	1.54	0.098
$\nu_\beta(CD_3)$	0.195	–0.45	0.116
ν(CF)	0.257	5.48	0.307
ν_σ		–0.99	–0.168
ν(HCl)	0.123	1.06	0.224

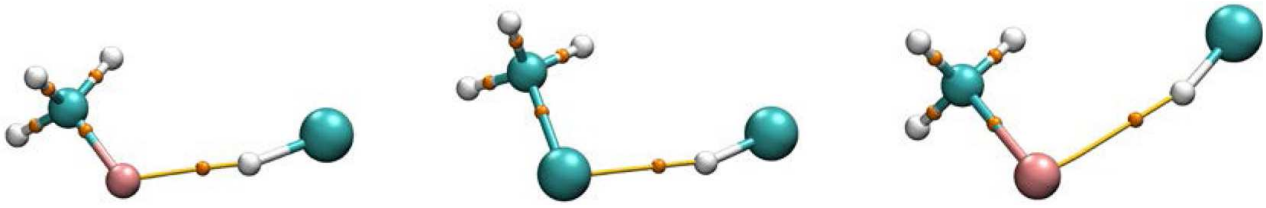

a *b* *c*

Fig. 6. Bond critical points (BCPs) in the complexes: $CD_3F\cdots HCl$ (*a*), $CD_3Cl\cdots HCl$ (*b*), and $CD_3Br\cdots HCl$ (*c*), obtained from AIM topological analysis

Table 8. **Results of AIM (Atoms in Molecules) analysis**

Complex	Bond	$\rho(r_{BCP})$ (a.u)	$\nabla^2\rho(r_{BCP})$ (a.u)	$G(r_{BCP})$ (a.u)	$-V(r_{BCP})$ (a.u)	$H(r_{BCP})$ (a.u)	$-E_{HB}$ (kcal/mol)
$CD_3F\cdots HCl$	$H\cdots F$	0.0220	0.0916	0.0217	0.0206	0.0011	5.52
$CD_3Cl\cdots HCl$	$H\cdots Cl$	0.0184	0.0554	0.0128	0.0118	0.0010	3.20
$CD_3Br\cdots HCl$	$H\cdots Br$	0.0166	0.0454	0.0105	0.0096	0.0009	2.57

Note: $\rho(r_{BCP})$ – density of all electrons, $\nabla^2\rho(r_{BCP})$ – Laplacian of electron density, $G(r_{BCP})$ – Lagrangian kinetic energy, $V(r_{BCP})$ – potential energy density, $H(r_{BCP})$ – energy density, $_{HB}$ – hydrogen bond energy.

This trend clearly demonstrates that the hydrogen bond strength in these complexes correlates with the electron-withdrawing ability of the halogen atom.

The table summarizes key topological parameters at the bond critical points (BCPs), including electron density $\rho(r)$, its Laplacian $\nabla^2\rho(r)$, and related descriptors used to evaluate the characteristics of the hydrogen bonds in the complexes.

The observed red shifts in the ν(HCl) stretching bands of the $CD_3Hal\cdots HCl$ complexes indicate the formation of weak hydrogen bonds, in agreement with previous theoretical studies. As highlighted by Calhorda [42], weak hydrogen bonding leads to characteristic vibrational frequency shifts that correlate with bond strength. Our MP2/anharmonic calculations and AIM analysis confirm this behavior, showing that the hydrogen bond energies in these complexes are small ($E_{HB} \approx$ 1–5.5 kcal $\cdot$ mol^{-1}) but sufficient to produce measurable spectral effects. These findings are consistent with the theoretical framework established for weak hydrogen bonds and provide further insight into the role of halogen substitution in modulating hydrogen bond properties.

Given that these complexes involve weak hydrogen bonds, the hydrogen bond energy (E_{HB}) was evaluated empirically by applying the approach proposed by Espinosa *et al.* [43], as expressed in equation (1). In this method, E_{HB} is correlated with the potential energy density V(r) at the bond critical point (BCP), providing a reliable way to estimate the interaction energy from AIM topological parameters.

$$E_{HB} \approx 0.429 \cdot V(r_{BCP}). \quad (1)$$

According to the AIM analysis results (Table 8), the values of $\rho(r_{BCP})$ at the hydrogen-bonded BCPs (Figure 6) and the corresponding hydrogen bond energies (E_{HB}) follow the trend $CD_3F\cdots HCl > CD_3Cl\cdots HCl > CD_3Br\cdots HCl$. As shown in Figure 4, the electronegativity (χ) of the proton-acceptor atoms involved in the intermolecular interactions satisfies the relation F > Cl > Br. The present study thus demonstrates that the correlation $E_{HB} \sim \chi$ is valid for these complexes based on AIM analysis.

5. Conclusion

This work demonstrates that $CD_3Hal\cdots HCl$ (Hal = F, Cl, Br) complexes form weak hydrogen bonds in liquid argon, which can be reliably detected by infrared spectroscopy. Systematic red shifts in the ν(HCl) absorption band were observed, increasing from fluorine to bromine, consistent with the decreasing proton-acceptor strength.

Anharmonic MP2 calculations reproduced the experimental spectral shifts, while AIM topological analysis confirmed the presence of weak hydrogen

bonds with interaction energies ranging from 2.6 to 5.5 kcal $\cdot$ mol^{-1}. A clear correlation between halogen electronegativity and hydrogen bond strength was established, in agreement with previous spectroscopic and theoretical studies.

The combined use of cryogenic liquid-argon IR spectroscopy and high-level quantum chemical calculations provides a robust methodology for probing weak intermolecular interactions. These findings not only extend earlier results on fluorinated hydrogen-bonded systems but also emphasize the role of halogen substitution in tuning the strength and spectroscopic signatures of hydrogen bonds.

1. A. Vasylieva, I. Doroshenko, S. Stepanian, L. Adamowicz. The influence of low-temperature argon matrix on embedded water clusters. A DFT theoretical study. *Low Temp. Phys.* **47**, 242 (2021).
2. I. Doroshenko, M. Onuk, A. Nekboev, B. Kuyliev. Influence of an argon matrix on trapped ethanol clusters. *Low Temp. Phys.* **51**, 480 (2025).
3. E.N. Kozlovskaya, I.Y. Doroshenko, V.E. Pogorelov, Y.V. Vaskivskyi, G.A. Pitsevich. Comparison of degrees of potential-energy-surface anharmonicity for complexes and clusters with hydrogen bonds. *J. Appl. Spectrosc.* **84**, 929 (2018).
4. I. Doroshenko, T. Rudenok, A. Lesiuk, A. Smal, O. Dmytrenko, L. Davtian, A. Drozdova. Peculiarities of ibuprofen interaction with polyethylene glycol polymer matrix. *Low Temp. Phys.* **51**, 215 (2025).
5. S.J. Grabowski. What is the covalency of hydrogen bonding? *Chem. Rev.* **111**, 2597 (2011).
6. P. Banerjee, T. Chakraborty. Weak hydrogen bonds: Insights from vibrational spectroscopic studies. *Int. Rev. Phys. Chem.* **37**, 83 (2018).
7. A. Lopez-Calvo, C.E. Manzanares. Vibrational overtone spectroscopy of saturated hydrocarbons dissolved in liquefied Ar, Kr, Xe, and N? *J. Phys. Chem. A* **112**, 1730 (2008).
8. W.A. Herrebout, B.J. Van der Veken, A. Medina, A.C. Hernández, M.O. Bulanin. Experimental and theoretical study of the far-infrared spectra of HCl dissolved in liquid Ar, Kr, and Xe. *Mol. Phys.* **96**, 1115 (1999).
9. I.M. Ismail. Cross-sectional areas of adsorbed nitrogen, argon, krypton, and oxygen on carbons and fumed silicas at liquid nitrogen temperature. *Langmuir* **8**, 360 (1992).
10. S. Moitra, S.K. Seth, T. Kar. Synthesis, crystal structure, characterization and DFT studies of L-valine L-valinium hydrochloride. *J. Cryst. Growth* **312**, 1977 (2010).
11. Z.A. Latajka, S. Scheiner. Structure, energetics, and vibrational spectrum of H_2O–HCl. *J. Chem. Phys.* **87**, 5928 (1987).
12. W.A. Herrebout, J. Van Gils, B.J. Van der Veken. A cryospectroscopic study of the oligomers of deuterium chloride in liquid argon, liquid krypton and in liquid nitrogen. *J. Mol. Struct.* **563**, 249 (2001).
13. R. Szostak, W.A. Herrebout, B.J. van der Veken. On the HCl and DCl complexes of methylenecyclopropane in liquid argon. *Phys. Chem. Chem. Phys.* **2**, 3983 (2000).
14. L. Andrews, X. Wang, Z. Mielke. Infrared spectrum of the $H_3N{-}HCl$ complex in solid Ne, Ne/Ar, Ar, and Kr. Matrix effects on a strong hydrogen-bonded complex. *J. Phys. Chem. A* **105**, 6054 (2001).
15. L.A. Zhigula, V.A. Kondaurov, I.S. Fedorov, D.N. Shchepkin. Study of anharmonic effects in the IR spectrum of a solution of CF_3Br in liquid argon. *Opt. Spectrosc.* **103**, 603 (2007).
16. J.C. Howard, J.L. Gray, A.J. Hardwick, L.T. Nguyen, G.S. Tschumper. Getting down to the fundamentals of hydrogen bonding: Anharmonic vibrational frequencies of $(HF)_2$ and $(H_2O)_2$ from ab initio electronic structure computations. *J. Chem. Theory Comput.* **10**, 5426 (2014).
17. K.E. Riley, J.A. Platts, J. Rezac, P. Hobza, J.G. Hill. Assessment of the performance of MP2 and MP2 variants for the treatment of noncovalent interactions. *J. Phys. Chem. A* **116**, 4159 (2012).
18. R.A. Bachorz, F.A. Bischoff, S. Höfener, W. Klopper, P. Ottiger, R. Leist, S. Leutwyler. Scope and limitations of the SCS-MP2 method for stacking and hydrogen bonding interactions. *Phys. Chem. Chem. Phys.* **10**, 2758 (2008).
19. V. Tognetti, L. Joubert. Density functional theory and Bader's atoms-in-molecules theory: Towards a vivid dialogue. *Phys. Chem. Chem. Phys.* **16**, 14539 (2014).
20. E. Espinosa, E. Molins. Retrieving interaction potentials from the topology of the electron density distribution: The case of hydrogen bonds. *J. Chem. Phys.* **113**, 5686 (2000).
21. A. Oranskaia, J. Yin, O.M. Bakr, J.L. Brédas, O.F. Mohammed. Halogen migration in hybrid perovskites: The organic cation matters. *J. Phys. Chem. Lett.* **9**, 5474 (2018).
22. S.J. Grabowski. Hydrogen bonding strength–measures based on geometric and topological parameters. *J. Phys. Org. Chem.* **17**, 18 (2004).
23. P. Politzer, J.S. Murray, T. Clark. Halogen bonding and other σ-hole interactions: A perspective. *Phys. Chem. Chem. Phys.* **15**, 11178 (2013).
24. G. Cavallo, P. Metrangolo, R. Milani, T. Pilati, A. Priimagi, G. Resnati, G. Terraneo. The halogen bond. *Chem. Rev.* **116**, 2478 (2016).
25. O.K. Voitsekhovskaya, D.V. Volkov, D.E. Kashirskii, V. Korchikov. Determination of spectral width of laser lines in the IR range using the absorption spectroscopy method. *Quant. Electron.* **42**, 634 (2012).
26. M. Lepère, O. Browet, J. Clement, B. Vispoel, P. Allmendinger, J. Hayden, M. Mangold. A mid-infrared dual-comb spectrometer in step-sweep mode for high-resolution molecular spectroscopy. *J. Quant. Spectrosc. Radiat. Transf.* **287**, 108239 (2022).
27. N. Montoya-Escobar, D. Ospina-Acero, J.A. Velásquez-Cock, C. Gómez-Hoyos, A. Serpa Guerra, P.F. Gañan Rojo, P.M. Stefani. Use of Fourier series in X-ray diffrac-

tion (XRD) analysis and Fourier-transform infrared spectroscopy (FTIR) for estimation of crystallinity in cellulose from different sources. *Polymers* **14**, 5199 (2022).
28. H. Lu, Y. Tian, R. Ma. Assessment of order of helical structures of retrograded starch by Raman spectroscopy. *Food Hydrocoll.* **134**, 108064 (2023).
29. M.J. Frisch *et al. Gaussian 16, Revision C.01* (Gaussian Inc., 2019).
30. G. Nurmurodova, G. Murodov, U. Khujamov, M. Buturlimova. Calculation of spectroscopic parameters of hydrogen and halogen bounded $CH_3CHO\cdots HF$ and $CH_3COH\cdots FH$ complexes. *Uzbek. Phys. J.* **24**, 310 (2022).
31. J. Krupa, M. Wierzejewska, J. Lundell. Experimental FTIR-MI and theoretical studies of isocyanic acid aggregates. *Molecules* **28**, 1430 (2023).
32. M.M. Kabanda, I. Bahadur. A DFT and MP2 mechanistic and kinetic study on hypohalogenation reaction of cysteine and N-acetylcysteine in aqueous solution. *J. Mol. Liq.* **349**, 118191 (2022).
33. R. Dennington, T.A. Keith, J.M. Millam. *GaussView. Version 6.1* (Semichem Inc., 2016).
34. G.A. Zhurko. *Chemcraft* – graphical program for visualization of quantum chemistry computations (2005) [https://chemcraftprog.com].
35. R.F.W. Bader. Atoms in molecules. *Acc. Chem. Res.* **18**, 9 (1985).
36. T. Lu, F. Chen. Multiwfn: A multifunctional wavefunction analyzer. *J. Comput. Chem.* **33**, 580 (2012).
37. W. Humphrey, A. Dalke, K. Schulten. VMD: Visual molecular dynamics. *J. Mol. Graph.* **14**, 33 (1996).
38. G. Nurmurodova, I. Doroshenko, G. Murodov, U. Khujamov. New FTIR and DFT study of $(CH_3)_2CO\cdots HCl$ hydrogen-bonded complex. *Ukr. J. Phys.* **70**, 381 (2025).
39. R. West, D.L. Powell, L. S. Whatley, M.K. Lee, P. von R. Schleyer. The relative strengths of alkyl halides as proton acceptor groups in hydrogen bonding. *J. Am. Chem. Soc.* **84**, 3221 (1962).
40. D.A.K. Jones, J.G. Watkinson. Infrared studies of the hydrogen bonding of phenolic hydroxyl groups. Part I. Intermolecular bonding to halogen atoms. *J. Chem. Soc.* 2366 (1964).
41. A.J. Barnes. Molecular complexes of the hydrogen halides studied by matrix isolation infrared spectroscopy. *J. Mol. Struct.* **100**, 259 (1983).
42. M.J. Calhorda. Weak hydrogen bonds: theoretical studies. *Chem. Commun.* **10** (10), 801 (2000).
43. E. Espinosa, E. Molins, C. Lecomte. Hydrogen bond strengths revealed by topological analyses of experimentally observed electron densities. *Chem. Phys. Lett.* **285**, 170 (1998).

Received 30.09.25

Г. Муродов, І. Дорошенко,
Г. Хушвактов, У. Худжамов, Г. Нурмуродова

СЛАБКИЙ ВОДНЕВИЙ ЗВ'ЯЗОК У КОМПЛЕКСАХ $CD_3Hal\cdots HCl$: ІЧ СПЕКТРОСКОПІЯ ТА РОЗРАХУНКИ МЕТОДОМ MP2

Утворення та коливальні властивості комплексів $CD_3Hal\cdots HCl$ (Hal = F, Cl, Br) досліджувалися в рідкому аргоні при температурі 120 K за допомогою інфрачервоної (ІЧ) спектроскопії та розрахунків ангармонічних частот на рівні MP2/6-311++G(3df,3pd). Після утворення комплексу валентна смуга ν(HCl) демонструвала систематичні червоні зміщення, що збільшувалися від CD_3F до CD_3Br, а також звуження завдяки зменшенню свободи обертання зв'язаного HCl. Для комплексу $CD_3F\cdots HCl$ додаткові червоні зміщення на 16 та 12 $см^{-1}$ спостерігалися в модах ν(CF) та $\nu_\beta(CD_3)$ відповідно, що узгоджується з результатами розрахунків. Аналіз розподілу заряду виявив зміни у його геометрії, що узгоджуються зі складними нелінійними структурами. Для раціонального пояснення варіацій спектральної інтенсивності були розраховані силові константи та приведені маси. Топологічний аналіз методом AIM (Atoms in Molecules) підтвердив слабкі водневі зв'язки з енергіями від 2,6 до 5,5 ккал/$моль^{-1}$, що корелює з електронегативністю галогенів (F > Cl > Br). Узгодженість між експериментальними та теоретичними результатами підкреслює зв'язок між коливальними зсувами, силою зв'язку та електронною структурою в системах зі слабкими водневими зв'язками.

Ключові слова: дейтеровані метилгалогеніди, водневий зв'язок, інфрачервона спектроскопія, рідкий аргон, розрахунки методом MP2, спектральні зсуви, слабкі міжмолекулярні взаємодії.